



OPEN

Influence of osteoporosis on the compressive properties of femoral cancellous bone and its dependence on various density parameters

F. Metzner^{1,2,3,5}✉, C. Neupetsch^{1,2,5}, J.-P. Fischer^{3,4}, W.-G. Drossel^{1,2}, C.-E. Heyde^{3,4} & S. Schleifenbaum^{2,3,4}

Data collection of mechanical parameters from compressive tests play a fundamental role in FE modelling of bone tissues or the developing and designing of bone implants, especially referring to osteoporosis or other forms of bone loss. A total of 43 cylindrical samples ($\varnothing 8 \times 16$ mm) were taken from 43 freshly frozen proximal femora using a tenon cutter. All femora underwent BMD measurement and additionally apparent- and relative- and bulk density (ρ_{app} , ρ_{rr} , ρ_b) were determined using samples bordering the compressive specimen on the proximal and distal regions. All samples were classified as "normal", "osteopenia" and "osteoporosis" based on the DEXA measurements. Distal apparent density was most suitable for predicting bone strength and BMD. One novel aspect is the examination of the plateau stress as it describes the stress at which the failure of spongy bone progresses. No significant differences in mechanical properties (compressive modulus E ; compressive stress σ_{max} and plateau stress σ_p) were found between osteopenic and osteoporotic bone. The results suggest that already in the case of a known osteopenia, actions should be taken as they are applied in the case of osteoporosis. A review of the literature regarding extraction and testing methods illustrates the urgent need for standardized biomechanical compressive material testing.

The demands on implants are steadily increasing especially in regard to primary stability, i.e. the anchoring quality in the bone immediately after implantation. Particularly in case of pathological or age-related loss of bone strength such as osteoporosis, precise knowledge of the mechanical bone properties, based on clinical diagnostics is of crucial importance for selecting a suitable implant. Osteoporosis is a systemic disease associated with lower bone mass and degeneration of the microarchitecture of bone tissue leading to a reduction in mechanical strength and fracture resistance. It is usually diagnosed by a radiological examination of the lumbar spine and proximal femur using the dual-energy X-ray absorptiometry (DEXA). Based on measured bone mineral content (BMD [g/cm^2]), the T-score is calculated as the deviation of the patient's BMD from a healthy control group. A distinction is made between normal ($t > -1$), osteopenia ($-1 > t > -2.5$), and osteoporosis ($t < -2.5$). Assigning the mechanical properties of a particular bone region to one of these standard categories may help to further develop numerical or physical bone models¹.

The base of all bone models, whether numerically or artificially produced, is fundamental information about the mechanical properties of the bone, which must be determined experimentally using donor tissues. Human bone tissue exhibits a high variance of mechanical properties due to different loading situation and geometries. For this reason, the compliance with a uniform methodology for the experimental determination of mechanical bone properties is of utmost importance. A widely used method for determining the mechanical properties of

¹Professorship for Adaptronics and Lightweight Design in Production, Institute for Machine Tools and Production Processes, Chemnitz University of Technology, Chemnitz, Germany. ²Fraunhofer Institute for Machine Tools and Forming Technology, Dresden, Germany. ³ZESBO - Center for Research On Musculoskeletal Systems, Department of Orthopaedic Surgery, Traumatology and Plastic Surgery, Leipzig University, Semmelweisstraße 14, 04103 Leipzig, Germany. ⁴Department of Orthopedic Surgery, Traumatology and Plastic Surgery, Leipzig University, Leipzig, Germany. ⁵These authors contributed equally: F. Metzner and C. Neupetsch. ✉email: florian.metzner@zesbo.de

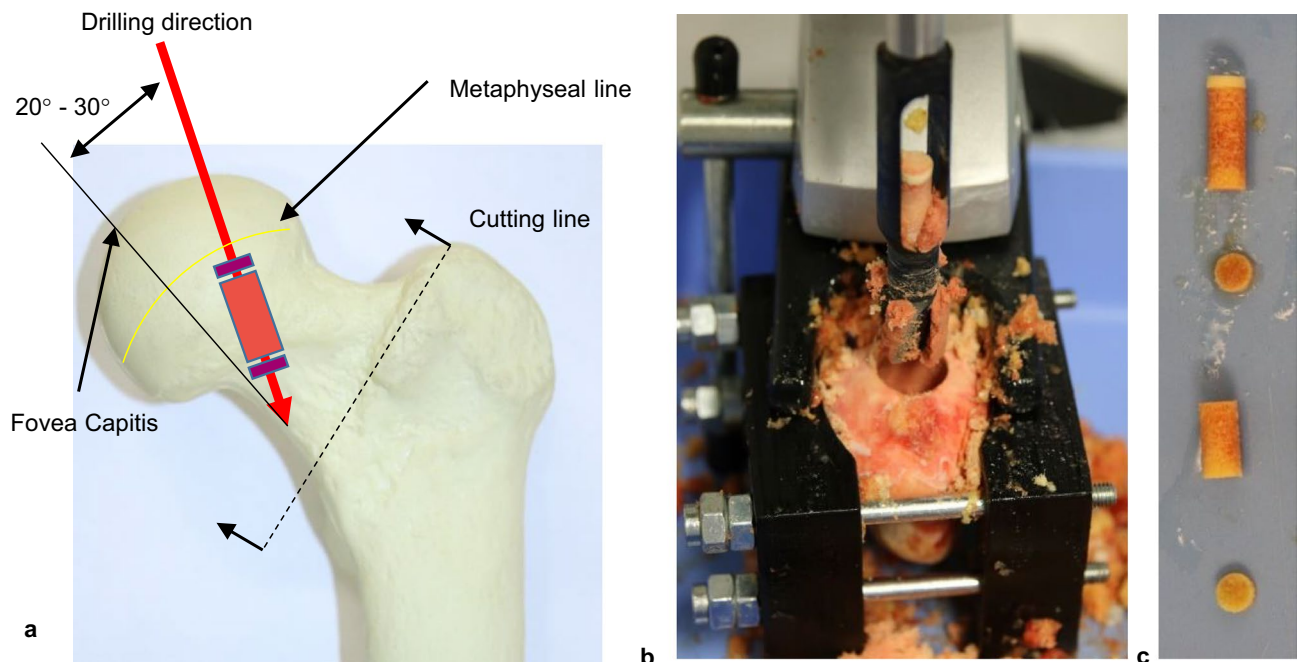


Figure 1. Specimen preparation: (a) shows the location of the samples within the available bone region. The drill penetrates into the diaphysis with an angle of 20° – 30° in lateral direction, starting from the fovea capitis. In (b) a femoral head fixed in the clamping jaws can be seen immediately after drilling. The fovea capitis is visible in (b) as a yellow and dark red spot below the drill hole. The already cut drill core can be seen in (c). The parts are arranged from proximal (top) to distal (bottom).

human bone tissue is the compression test². Despite the immense number of such examinations, no standardized protocol (ISO, ASTM, etc.) with specified process parameters has been established so far. For this reason, the data obtained from various studies are comparable only to a limited extent. An essential problem is the sparse information on how to take tissue samples. One aspect for standardization is the determination of the density parameters since they have great influence on bone strength^{3,4}. The aim of the study is the description of similarities and differences in the methodological approach in the performance of compressive testing of human cancellous bone. Furthermore compressive tests will be conducted with the aim of referring the experimental mechanical and morphological parameters to clinical categories of osteoporosis.

Materials and methods

Specimen preparation technique. 41 femoral heads from 26 human cadavers (21 females, 20 males) with mean age of 80.7 ± 10.9 years were obtained in fresh and anatomically unfixed condition. All body donors gave their informed and written consent to the donation of their bodies for teaching and research purposes while alive. Being part of the body donor program regulated by the Saxonian Death and Funeral Act of 1994 (third section, paragraph 18 item 8), institutional approval for the use of the post-mortem tissues of human body donors was obtained from the Institute of Anatomy, University of Leipzig. The authors declare that all experiments were conducted according to the principles of the Declaration of Helsinki. All bones underwent DEXA measurement for determination of bone mineral density (BMD). Based on the clinically determined T-scores all specimen were classified according to the definition specified by WHO as “normal” (N=9), “osteopenia” (N=20) and “osteoporosis” (N=10). Due to inserted hip endoprosthesis two femurs could not be included in the study which leads to a total number of specimen of N=39. All bones were stored fresh frozen at -83°C until further preparation.

The femoral heads were separated from the remaining bone according to the procedure for inserting a hip endoprosthesis. The separation line runs through the femoral neck one to two centimetres distally to the femoral head. The removal of the drill cores was carried out with a tenon cutter (FAMAG Series 1616, FAMAG-Werkzeugfabrik GmbH & Co. KG, Remscheid, Germany) and a stationary drilling machine (model PBD 40; Robert Bosch GmbH Power Tools, Leinfelden-Echterdingen, Germany) in superior-inferior direction along the trabecular alignment in the femoral neck as displayed in Fig. 1a.

To align the drilling direction with the main trabecular orientation the bones were clamped in self-constructed and 3d printed jaws (see Fig. 1b). There were conical cut-outs on the inside of the jaws to prevent the bones from slipping. The still frozen femoral heads were placed on a lying jaw by hand. Using the tendon attachment of the ligamentum caput femoris as guidance the head was inserted with the drilling direction parallel to the frontal plane. Afterwards, the bone was tilted so that the drilling direction (see Fig. 1a) was orthogonal to the upper edge of the clamping jaw. The samples are cut to size with a diamond band saw (EXAKT 310, EXAKT Advanced Technologies GmbH, Norderstedt) to ensure parallel end faces. The drill cores are fixed again in 3d printed jaws (see Fig. 2 right) during the sawing process. Orthogonal end faces could be provided due to fixation of the jaws

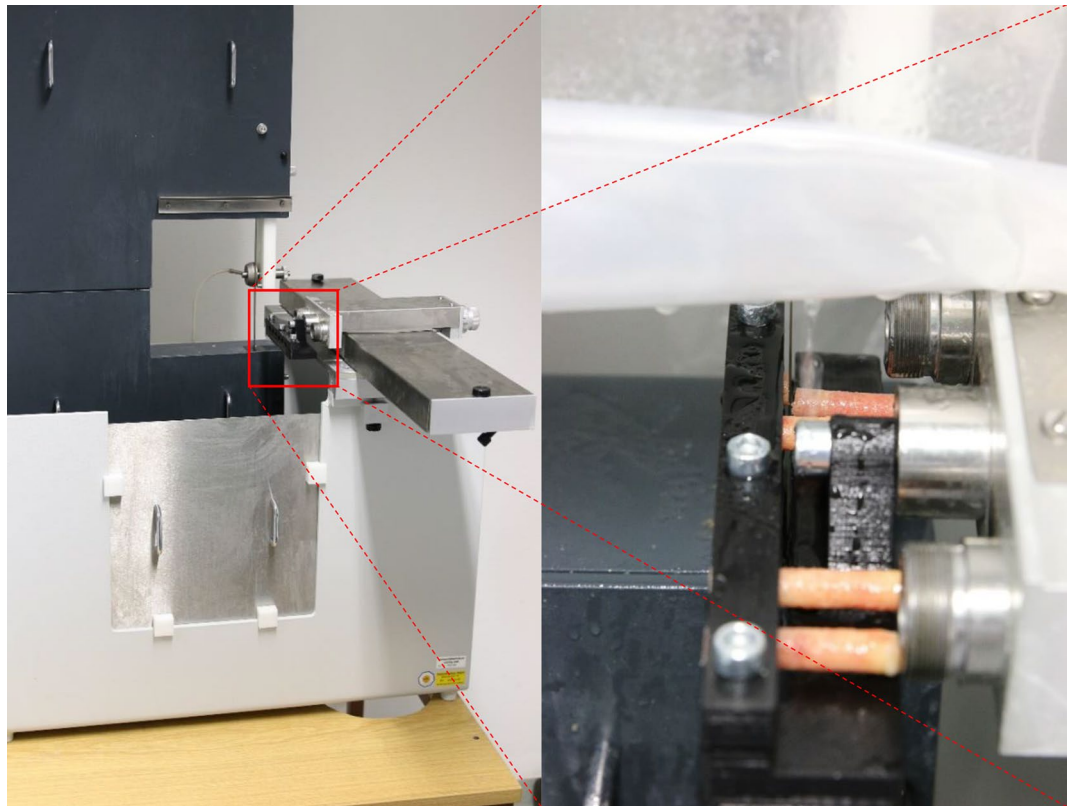


Figure 2. Self constructed and 3D printed clamping jaws are mounted at the parallel guidance of the band saw. The mounted section of the drill core is later used as mechanical specimen. Sawing was carried out under permanent water irrigation.

to the parallel guide in the band saw. The drill cores were clamped in the areas, which were later mechanically tested, in order to avoid misalignment due to re-clamping. A sample geometry of $\text{Ø } 8 \times 16 \text{ mm}$ is used for all mechanical specimens. In previous studies, as seen in Table 3, a diameter of 8 mm is commonly used as it is wide enough to include enough trabecular connections⁵. The length ratio of diameter to length of 1:2 is specified and recommended in DIN ISO 50134⁶ and therefore was implemented in the present study.

Two slices of 2 mm thickness were cut from the drill core for density determination (see Fig. 1c). Each of the slices originated from the areas bordering the mechanical specimen proximally/distally. These slices were defatted by a 5-day ethanol storage at 4 °C followed by three days storage in NaCl-solution (0.9%) at 21 °C. The following density parameters were then measured according to the Archimedeian principle with ethanol as density medium using a precision scale with integrated density kit (Mettler-Toledo GmbH, Gießen, Germany, Model ML303T/00). Apparent density ρ_{app} was determined from bone mass and sample volume. Bulk density ρ_b is calculated from bone mass and bone volume. Additionally the relative density ρ_r was calculated by the ratio of defatted bone volume and the sample volume. The nominal geometry of all samples is measured with a calliper gauge. Sample length and diameter of the discs is determined at one measuring point. The diameter of the specimen used for pressure tests is determined as the average of three measuring points. In between all processing steps the samples are stored in physiological saline solution to avoid dehydration.

Mechanical testing. The compression tests were carried out on a servo-electric single-axis testing machine (INSTRON GmbH, Darmstadt, Germany). The force was recorded by a force transducer (measuring range 2 kN) and the strain measurement was performed via the machine traverse. Machine compliance was not adjusted. The force was applied via two plane-parallel anvils. Before each test, the test surfaces were cleaned and moistened with Ringer's solution to minimize friction on the contact surfaces. The testing procedure starts with the application of the preload of 10 N before going through a hysteresis loop for pre-conditioning according to⁶. Therefore the test force is increased up to an equivalent stress value of $\sigma_1 = 3.2 \text{ MPa}$ and subsequently released to $\sigma_2 = 1.6 \text{ MPa}$. After passing through the hysteresis loop once the anvil continues and compresses the specimen until a total distance of 12 mm is reached or the measuring range of the force transducer is exceeded. The reversal points of the hysteresis loop result from the mean plateau stress of a pre-test series with $n = 5$ specimens ($\sigma_1 = 0.2 * \sigma_p$; $\sigma_2 = 0.4 * \sigma_p$ ⁶). According to⁶ plateau stress σ_p is defined as the mean value of the stresses between $\varepsilon = 20\%$ and $\varepsilon = 40\%$. This value marks the average stress of failure progression after initial structural collapse. Up to a deformation of 10%, the test is performed at a test speed of $v_1 = 0.016 \text{ mm/s}$, then $v_2 = 0.16 \text{ mm/s}$ for a sufficiently high sampling rate in the linear range to ensure accurate values determining the compressive modulus.

Then the test speed is increased to $v_2 = 0.16$ mm/s in order to save time in the plateau range. From the measured values, the parameters plateau stress σ_p , compressive stress σ_{max} and compressive modulus E are determined. The compressive stress σ_{max} is the stress value of the first maximum in the curve which marks the initial structural failure. In literature this value is often called ultimate stress. E is determined using the mathematical slope formula for linear functions from the reversal points of the hysteresis. In case samples fail while passing through the hysteresis, the measurement is aborted after reaching σ_{max} . Then E is determined from the maximum gradient of the slope and no σ_p is determined. All measures were carried out within one day to avoid storage influences.

Statistical analyses. Descriptive statistics were examined using IBM SPSS Statistics 24 (IBM Corporation, Armonk, NY, USA). T-tests for independent samples were carried out between 5 different pairs of groups (male vs. female; left vs. right; normal vs. osteoporosis; normal vs. osteopenia; osteopenia vs. osteoporosis) for all measured structural and mechanical parameter. Statistical significance is defined with $p < 0.05$. Simple linear regression was used to determine relationships among density parameters. Regression between mechanical parameters and the density parameters was carried out by a power function.

Results

The mechanical samples ($n = 40$) have a diameter of $d = 8.12 \text{ mm} \pm 0.07 \text{ mm}$, a length of $L = 15.98 \pm 0.06 \text{ mm}$ and the density samples have a length of $L_s = 1.98 \text{ mm} \pm 0.05 \text{ mm}$. The mean BMD of 0.69 g/cm^2 lead to an average T-score of -1.69 . Average values as well as their standard deviations are displayed in Fig. 3a–c for each distal and proximal bone slices, grouped into the previously defined stages of osteoporosis. The differences in the density values between the proximal and distal slices is around 0.02 g/cm^3 for ρ_b , 30% for ρ_r and 0.3 g/cm^3 for ρ_{app} . Relative and apparent densities of the distal slices are clearly lower than the proximal relatives. While the proximal bulk density falls significantly from “normal” to “osteopenia” ($p = 0.03$) and from “normal” to “osteoporosis” ($p = 0.01$), there is no significant difference between “osteopenia” and “osteoporosis” ($p = 0.76$). No significant differences were found between the distal bulk densities. The proximal relative density of “normal” specimen is not significantly higher than “osteopenia” ($p = 0.34$) but is significantly higher than “osteoporosis” ($p = 0.03$). The distal relative density drops significantly from normal “normal” to “osteopenia” ($p = 0.00$) and from “normal” to “osteoporosis” ($p = 0.00$), but not from “osteopenia” to “osteoporosis” ($p = 0.50$). An almost similar pattern is seen for the apparent density. The proximal apparent density drops significantly from “normal” to “osteopenia” ($p = 0.03$), from “normal” to “osteoporosis” ($p = 0.00$) and also from “osteopenia” to “osteoporosis” ($p = 0.03$). The distal apparent density drops significantly from “normal” to “osteopenia” ($p = 0.00$), from “normal” to “osteoporosis” ($p = 0.00$) but not from “osteopenia” to “osteoporosis” ($p = 0.49$).

Table 1 shows the R^2 values of simple linear regression analyses. The clinical parameters BMD and T-score are used as independent variables for explanation of the variances in each determined density measures. Highest R^2 values were found for the distal apparent density of the distal slices as displayed in Table 1. The model quality worked slightly better with the BMD as independent variable.

Figure 4 shows a typical stress–strain curve with a close-up on the initial force application. There is a toe region located at the beginning followed up by the hysteresis loop. The red line marks the turning points which defines the compressive modulus and fits nicely with the maximum slope of the linear region of the curve. Additionally, there was no visible plastic deformation after preconditioning.

All measured mechanical parameters are grouped similar to the previously displayed density measures as displayed in Fig. 5a–c. σ_{max} of “normal” bones ($14.1 \pm 7.3 \text{ MPa}$) is significantly higher ($p = 0.00$) than bones with “osteopenia” ($6.8 \pm 4.5 \text{ MPa}$, $p = 0.00$) and as bones with “osteoporosis” ($6.1 \pm 3.1 \text{ MPa}$, $p = 0.01$). The plateau stresses show comparable results. σ_p of “normal” bones ($11.3 \pm 3.5 \text{ MPa}$) is significantly higher than bones with “osteopenia” ($7.8 \pm 3.8 \text{ MPa}$; $p = 0.00$) and “osteoporosis” ($7.5 \pm 3.9 \text{ MPa}$; $p = 0.04$). The average difference of σ_p between “osteopenia” and “osteoporosis” is not significant ($p = 0.9$). There were no significant differences between the moduli of each group.

Regression analysis of the mechanical parameters (σ_{max} , σ_p , and E) with the all available density measures using a power function demonstrate that the distal apparent density shows highest R^2 values as seen in Table 2. Figure 6a–c show the previously mentioned plots of each mechanical parameter over the distal apparent density. The specimen of female donors has significantly lower T-score ($P = 0.00$), BMD ($P = 0.00$), $\rho_{r,distal}$ ($P = 0.01$), $\rho_{app,proximal}$ ($P = 0.02$) and $\rho_{app,distal}$ ($P = 0.00$) than the ones from male donors.

Discussion

Cylindrical samples were collected from the femoral neck with a drill along the main trabecular orientation. Directly distal to the epiphyseal line, three samples were cut from each drill core. A cylindrical specimen with a length to diameter ratio of 2:1 for mechanical testing and adjacent 2 mm discs were collected proximally and distally for examination of morphological parameters.

All density measures of both distal and proximal slices decreased with progressing osteoporosis. This is an obvious result as it is known that osteoporosis leads to bone loss and downgrade of trabecular architecture¹. But only $\rho_{r,proximal}$ and $\rho_{app,proximal}$ show a significant difference between osteoporotic and osteopenic specimen. There is just a slight difference in the bulk densities of about 0.5 g/cm^3 between the specimen location which underlines the effectiveness of the defatting method as the bone density should be the same over each drill core. By regression analysis using power function seen in Table 2 it was shown that the mechanical properties can be best explained by the apparent density of the distal slices. About 60% of the variance in σ_{max} can be explained by $\rho_{app,distal}$. It was found that the effectiveness of predicting the mechanical properties works best using the distal slices, which have the lower density values and therefore this region predicts some kind of predetermined breaking area within the mechanical specimen. The reason may simply be that areas with a low density will break

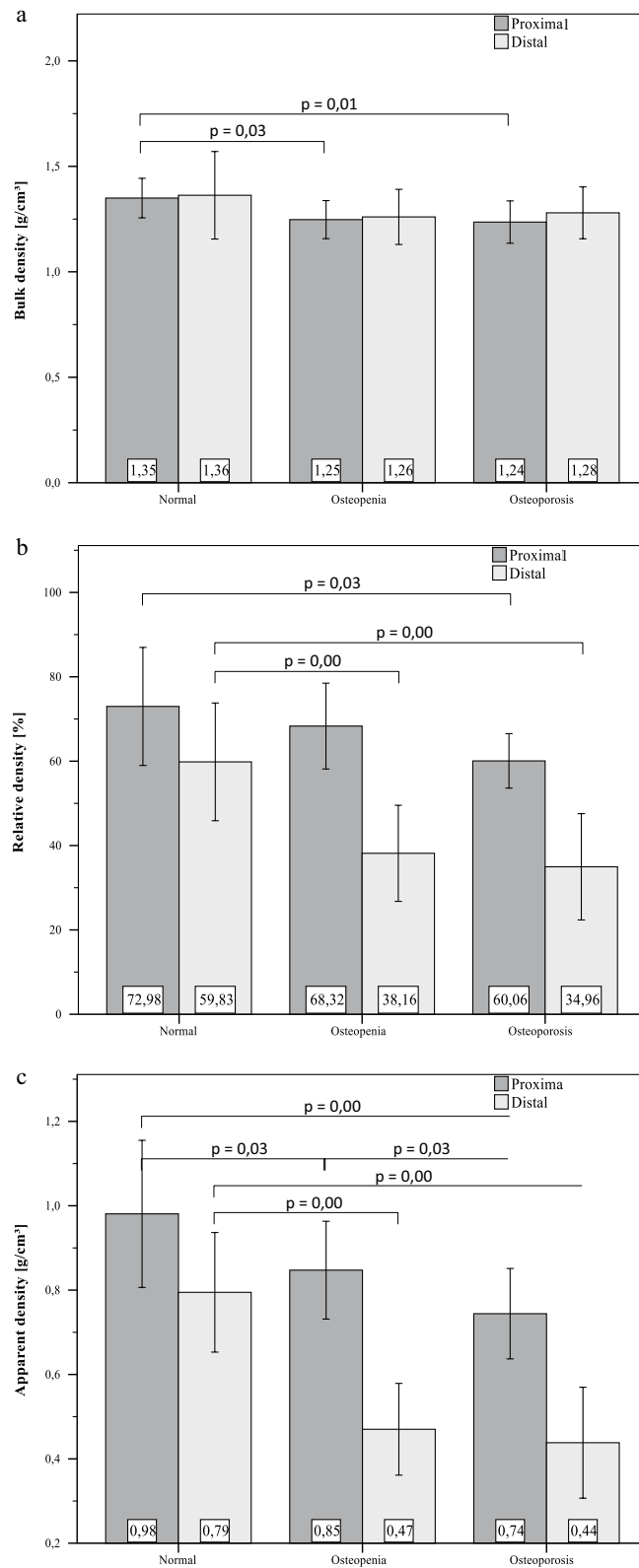


Figure 3. Mean density values of the density samples collected proximally and distally oriented to the mechanical specimen. The data grouped regarding WHO classification for osteoporosis based on BMD measurements of each donor bone. Bulk density ρ_b (a) stays roughly constant with low differences between sites. Apparent density ρ_{app} (b) and relative density ρ_r (c) show both great differences both between sites and groups. all significant differences are marked with their specific p-value from independent t-tests.

R ²	T-score	BMD
$\rho_{b,proximal}$	0.182*	0.160*
$\rho_{b,distal}$	0.068	0.044
$\rho_{r,proximal}$	0.105*	0.082
$\rho_{r,distal}$	0.327*	0.384*
$\rho_{app,proximal}$	0.244*	0.203*
$\rho_{app,distal}$	0.493*	0.543*

Table 1. R² values of linear regression analysis by plotting each measured density values over T-score and BMD. Significant models are marked with *.

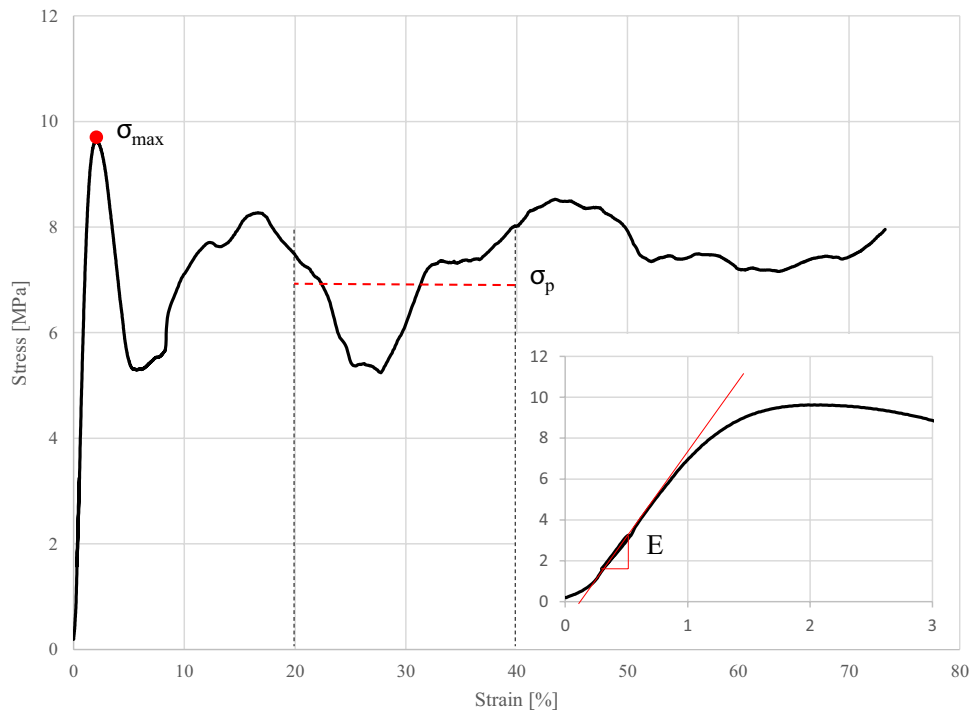


Figure 4. A typical stress–strain curve of one measured specimen is displayed. After a little toe region due to misalignment of the anvils and the specimen endfaces, the following linear region defines the compressive Modulus E and is nicely represented by the turning points of the hysteresis loop. After the first maximum σ_{max} which marks the initial structural failure the stress drops at first and continues with irregular swelling. Despite the high swelling amplitude the plateau stress agrees well with the average stress in the areas of high strains.

earlier than denser areas as described by⁷. The high explanatory accuracy of the mechanical parameters using separate discs works better than relating it to the outcome of DEXA measurement. The undescribed portions of data may be due to misalignment of the specimen axis and the main trabecular orientation. So, if there is found a simple way for determining the main trabecular orientation on the extracted specimens, the present method of density measurement may be an alternative for μ CT-scanning.

Also, the bone marrow may not be completely removed by the baths in ethanol and saline solution. Apparent and relative density rise therefore with increasing bulk-volume. This could be an explanation why the distal apparent density works best for prediction of BMD or mechanical parameters as seen in Tables 1 and 2. We assume that ρ_{app} is less susceptible to measurement errors than the other determined density parameters. If the bone marrow is not completely removed during defatting, the mass fraction of the marrow still contained in the sample is probably significantly smaller than the volume fraction of the said marrow. For the geometric density, the sample mass is related to the total sample volume, so only the mass and not the volume of the undissolved bone marrow is included. Therefore the same methodical error is taken less into account.

Using separate test specimens for density determination, no further processing of the mechanically tested specimens takes place apart from the extraction process. For that, the reducing influence of bone marrow on the compressive stress as said by⁸ was taken into account. The defatting of the bone is necessary for determining the bone density according to the Archimedean principle for the determination of bone mass. The defatting process is facilitated by the small dimensions of the density samples and the associated short diffusion paths.

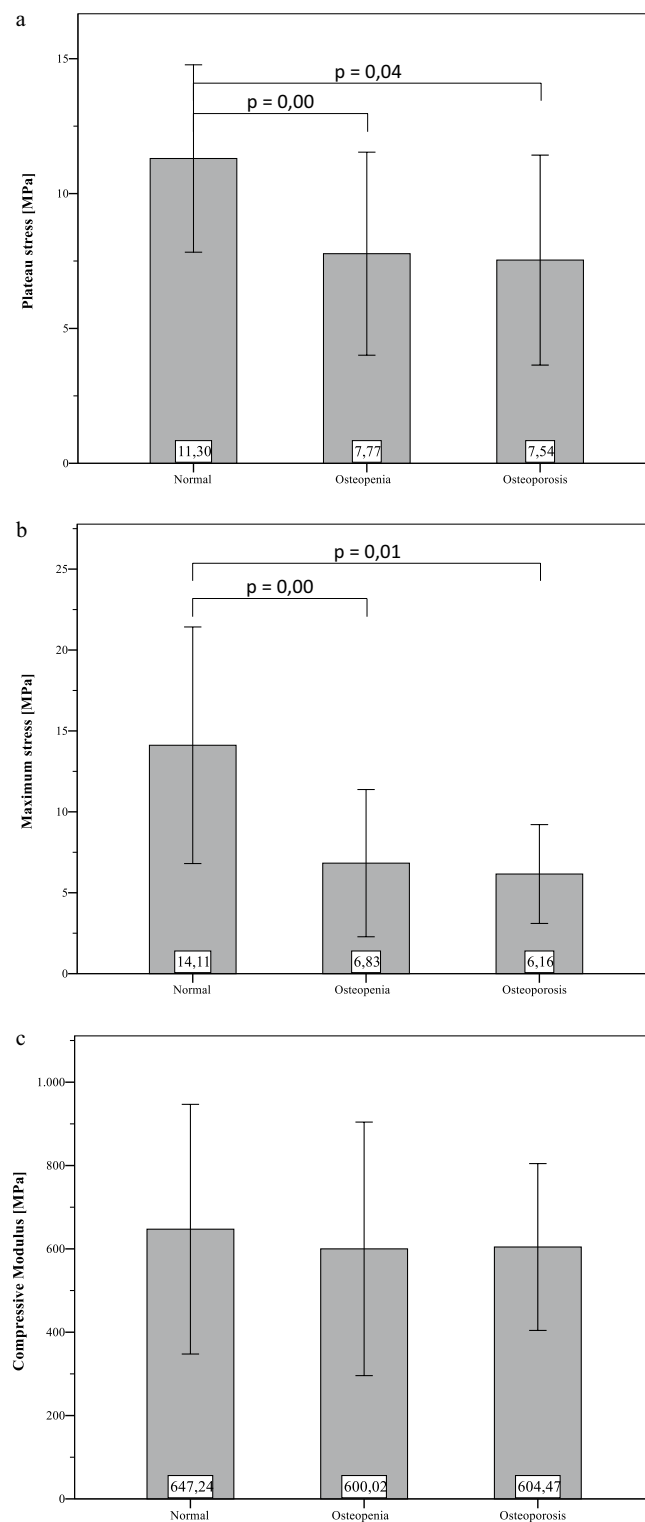


Figure 5. Mean values (with standard deviation) of the determined mechanical properties, grouped regarding WHO classification for osteoporosis based on BMD measurements of each donor bone. There are no significant differences in all mechanical properties (σ_p , σ_{max} , E) between “osteopenia” and “osteoporosis”. Significant differences within presented groups are marked with their specific p-value from independent t-tests.

By grouping the samples into the stages of osteoporosis it was shown that bone strength (σ_{max} , σ_p) generally decreases as osteoporosis progresses, whereas the modulus remains relatively constant at about 600 MPa for each

R ²	σ_p	σ_{max}	E
$\rho_{b,proximal}$	0.041	0.127*	0.033
$\rho_{b,distal}$	0.048	0.090	0.069
$\rho_{r,proximal}$	0.114	0.002	0.005
$\rho_{r,distal}$	0.079	0.392*	0.226*
$\rho_{app,proximal}$	0.198*	0.046	0.000
$\rho_{app,distal}$	0.161*	0.598*	0.360*
BMD	0.042	0.099	0.009

Table 2. R² values of regression analysis using power function. All three mechanical parameters can be best explained by distal apparent density. Significant models are marked with *.

group. The largest jump is visible in both maximum stress and plateau stress from "normal" to "osteopenic" bone. Although the samples classified as osteoporotic and osteopenic do not show significant differences. These results suggest that already in the case of a known osteopenia, actions should be taken as they are applied in the case of osteoporosis (e.g. cementation of implants, imaging techniques). The predictive power of the BMD decreases with younger patients⁹. Since the body donors from which the samples were obtained were on average very old, this question should be pursued further and the sample should be expanded accordingly.

It is interesting to note that the maximum stress of the "normal" specimens is on average about 2–3 MPa above the plateau stress. However, the plateau stress of the osteopenic and osteoporotic samples is about 1 MPa higher than the maximum stress. Thus, the initial failure stress of healthy bone is very high, while the forces required for progression of failure are comparatively low. This could be helpful for evaluating the primary stability of implants which are anchored mainly in trabecular bone, since e.g. the surrounding tissue initially fails while implanting bone screws therefore loosening is merely failure progression. It must also be taken into account that the test speed is increased by a factor of 10 after the maximum stress is exceeded. Consequently, the plateau stress could be underestimated due to the influence of the loading speed on the material stiffness. Carter and Hayes¹⁰ reported, that energy absorption increases at strain rates of minimum 10.0 per second. Also they found out, that both modulus and strength increase proportional to strain rate with a power of 0.06. Accordingly, this means that the tenfold increase in speed leads to an increase in modulus and strength by a factor of about 1.16. The extent to which this affects plateau stress cannot be precisely stated at this point. Though it is assumed that there is an influence, which is relatively small.

The plateau stress as it is found here has only been determined in a few studies in a comparable way. Halgrin et al.⁸ determined the plateau stress (σ_{mean}) as the mean stress between the compressive stress and an elongation value of 60%. They investigated cancellous bone from the bovine ribs. A very long plateau area was observed with stress values slightly below the compressive limit. Although the absolute stiffness values cannot be directly compared, the present study showed very similar post-yield behaviour. Fhyrie and Schaffler¹⁵ examined the post-yield behaviour up to an elongation of 15%. They determined the minimum stress that occurs after failure as a characteristic value. Interestingly, they found a significant correlation between stiffness and the minimum stress after failure.

In contrast to the post-yield behaviour of bovine bone examined by⁸, the present study recorded large fluctuations in the highly plastic range. Some curves show irregular swelling behaviour, which indicates an inhomogeneous structure within the samples. This could be explained as follows. As the weak zones collapse, the stress curve decreases. If the now compacted material hits a stronger zone, the stress rises again until next failure. This behaviour is repeated several times until the material is finally compacted.

The measured maximum stresses are even higher than the values determined in¹¹ for the identical bone region (yield strength: 6.7 MPa; compressive modulus 263 MPa). Nazarian et al.¹¹ used brass plates glued to the front sides of the specimens in order to eliminate transverse forces and to prevent buckling of the trabeculae at the interface. Also a ball joint was introduced to compensate for parallelism deviations, thus preventing underestimation of the bone strength in the axial direction. With this measurement setup the determined modulus should be higher than the moduli of the present study as the authors tested the same bone region and the mean age of the donors was the same on average. Additionally Nazarian et al. used an embedding system for prevention of end artefacts as described by¹².

Ciarelli et al.¹³, Morgan et al.¹⁴ and Perilli et al.¹⁵ tested cancellous bone from the identical bone region as the present study and obtained mean compressive stresses of around 15 MPa and matched very good with the "normal" group. With an average compressive modulus of 1100 MPa¹³ measured almost twice as high values as the present study. The compressive Modulus determined by¹⁴ where around 5 times higher. The present stiffness E should be interpreted with caution as the machine compliance was not taken into account. With the approximately known underestimation of the stiffness due to direct force application of around 40% mentioned by¹⁶ the real compressive modulus could be around 700 GPa or higher. The differences of the presented stiffness values compared to the literature can best be explained by the use of direct implantation of the testing force in the specimen. This leads to end-artefacts because the trabecular ends are not supported. The anvils were lubricated before testing, but end artefacts are the main explanation of the comparably low stiffness values. Nevertheless it is possible to point out differences within each group in terms of osteoporosis. One potential limitation of the present study is that it does not address or improve evaluation and assessment of fragility fractures. They occur

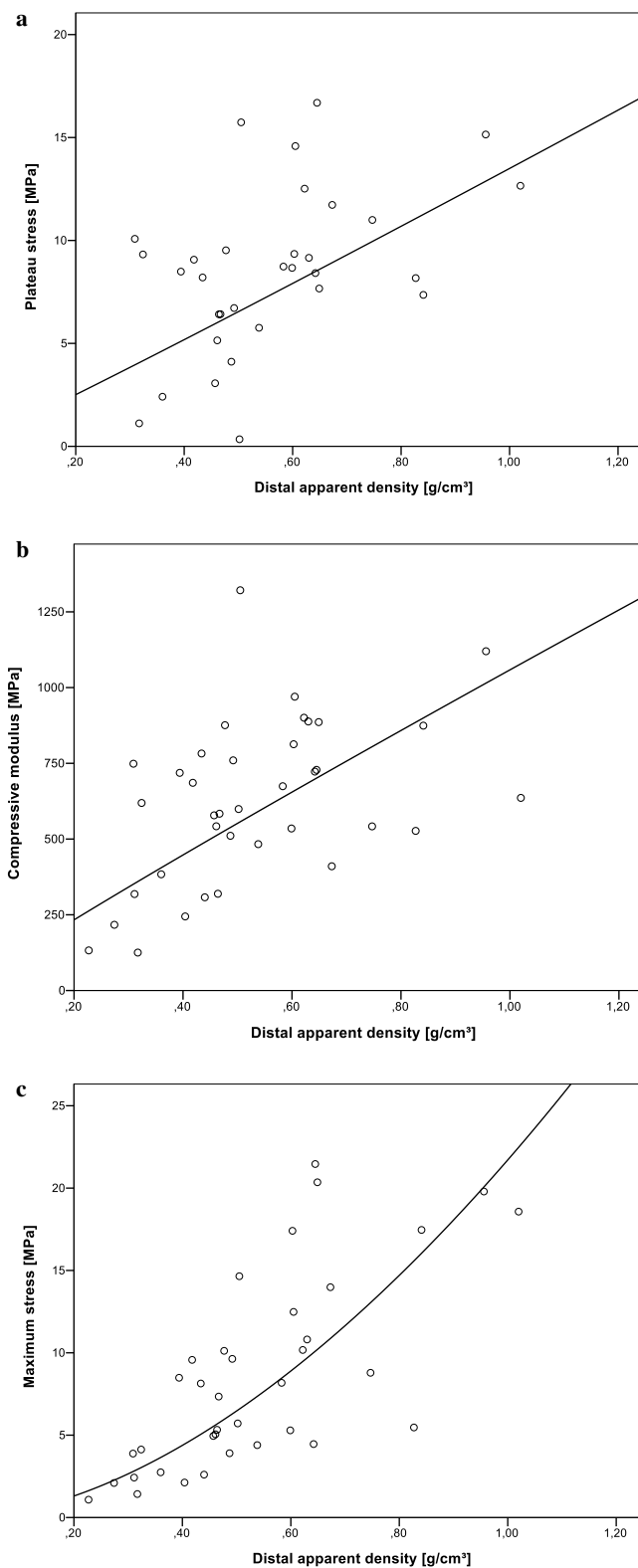


Figure 6. Mechanical properties plotted as power function over the distal apparent density showed best models according to R^2 values (s. Table 2).

in vivo on whole bones, whereas in this work isolated spongy bone specimen were examined. The aim was to provide an overview of previous methods for determining the mechanical parameters of bones in uniaxial

compression tests as well as comparing these to clinical outcomes like T-score, something that may or may not be clinically relevant as far as fragility fractures are concerned.

Due to the large differences in the mechanical properties of the identical anatomical region between different studies, an overview of different sampling and testing methods is shown below. Table 3 shows the methodological approach of a large number of studies arranged according to the bone region examined. Special attention was put on the method of specimen collection, specimen geometry, test protocol and recorded test parameters rather than on actually recorded results. This intends to illustrate the large discrepancy in the methodology of the current state of research. The listed studies represent only a fraction of all studies that investigate the compression behaviour of cancellous bone. Only those studies were selected which determine human bone properties in the uniaxial compression test.

When specimen are taken from bone parts, mechanical parameters are usually determined along the predominant trabecular alignment. Due to the strongly anisotropic material behaviour of the cancellous bone, the precise alignment of the bone tissue is of highest priority, since this step is fundamental for the informative value of the entire study.

Unfortunately, the extraction method and positioning of tissue is often described vaguely. In addition, there are numerous methodical approaches as displayed in Table 3. A diamond coated band saw is often used to cut discs from the bone, from which the drill cores are then removed perpendicular to the cutting plane with a trephine drill^{17,19,21,24,25}. Some determine the position of the section planes by means of trabecular alignment using imaging techniques such as contact X-rays or CT^{17,21}. Another method for aligning bone tissue is to embed the bones or bone segments in cast resin or plaster^{20,29}. Regardless of the procedure, during all of the above methods a bony object must be aligned manually at some point. The jaws used in this study for clamping and aligning bone tissue, in conjunction with the use of imaging techniques, represent a fast and flexible alternative to embedding, since the curing times involved are very time-consuming. Still one limitation is the alignment of the femoral heads in the clamping device, since the course of the trabecula is not exactly visible from the outside. At this point some improvements need to be done in future experiments.

Removing drill cores with a tenon cutter enables working without additional cooling medium due to allow heat accumulation. Normally, tenon cutter are used to create wooden plugs with fixed external dimensions which is very useful for mechanical testing. Furthermore, the used tool offers the opportunity to remove very long drill cores in comparison to ceramic drills. For evaluation purposes the drill cores were extracted from frozen bone. After extraction the cores showed no outer damages. Apart from that, the marrow was still in a frozen state and therefore supported the bone structure in between while drilling. Trephines or diamond coated drill cores are widely used for extracting cylindrical samples^{11,12,17,19,21,24,25}. The advantages of this tool are clean cutting surfaces and a small outer radius, which allows more specimens to be extracted from the limited space of a bone part. However, cooling is required during drilling to prevent tissue damage possibly caused by frictional heating. In addition, bone chip transport could prove to be problematic, since it can impair cooling at great drilling depths. The used tenon cutter provides an improved chip transport and a lower number of cutting edges resulting in less heat development. This eliminates the need for cooling during drilling. Furthermore, the tenon cutter enables the extraction of longer drill cores compared to the trephine.

Cutting the drill cores to size using the parallel guiding system of the band saw as well as a 3D printed clamping device leads to precise plane-parallel cutting end faces, which ensure uniform and centric force application into the sample. Still, small but unavoidable misalignment errors of the anvils led to minor initial toe regions.

The revised literature (see Table 3) contains mostly cube-shaped and cylindrical specimens with a width or diameter between 5 and 10 mm. The ratio of sample length to diameter varies between 1 and 2. This trend in the literature is based on the work of Linde et al.³⁰, who investigated the effect of sample geometry on mechanical behaviour and recommended a diameter of 7.5 mm for cylindrical samples. In the present study we used cylindrical specimens with a diameter of 8 mm. This diameter was chosen because it is most frequently found in literature (see Table 3) and additionally very close to diameter suggested by³⁰.

The mechanical properties of cancellous bone strongly depend on density^{4,31–35}, hence density determination is an essential part of biomechanical testing of bone tissue. The most frequently determined parameters include apparent density and bone volume fraction. The Archimedean principle and the high-resolution μ CT are the methods most widely used for this purpose as presented in Table 3. While density determination using the Archimedean principle appears to be quick and easy, the bone marrow must first be removed from the sample in a preceding step if information about the bone volume content is needed. There are various solutions for this process step, such as blowing out with an air jet, chemical dissolving, the use of ultrasound baths or the combination of several approaches^{19,20,36}. However, as the sample size increases and the pore size of the spaces decreases, this process becomes more difficult or more complex to perform due to larger diffusion paths.

The determination of bone density using μ CT is contactless, but requires a lot of effort. The accuracy of this method depends not only on the resolution but also on the determination and validation of a threshold value during segmentation¹⁹. A major advantage of μ CT analysis of extracted spongy bone specimen is the precise determination of structural parameters like trabecular thickness or trabecular connectivity. However, this method is very time and cost consuming compared to the much simpler submersion techniques. Another option would be QCT, as it can accurately determine the apparent density of the bone, and this value is well suited to predict the mechanical properties of cancellous bone. In clinical practice, this method is used less frequently than DXA due to the high radiation exposure to patients. For biomechanical analyses of bone, QCT could well be used instead of μ CT.

The way in which the test force is transferred to the specimen has a great influence on the mechanical properties. In older studies^{18,20,25} due to simplicity the test force was applied directly from the plane-parallel anvils into the specimen. Therefore the unsupported trabecular ends at the end faces are subjected to undesirable bending forces which lead to increased strain in the boundary areas of the specimen. As a consequence the stiffness of the

Region	Author	Specimen geometry					Testing protocol			Parameters	Scope of study (donors; specimen)
		Tools	Bone alignment	Specimen alignment	Density measurement	Specimen geometry	Preconditioning (Number of Cycles; upper Limit)	Force initiation	End of testing		
Proximal femur	Present study	T; B	C	SI	A	Cylinder (Ø 6 × 16 mm)	1; from pre study	D	ε = 70%	E, σ _{max} , σ _p	5; 10
	Ciarelli, Fyhrie et al. ¹³	B	I	SI	μCT	Cube (8 × 8 mm)	10; ε = 0.4%	D	ε = 15%	E, σ _{max}	58; 58
	Martens, van Audekercke et al. ¹⁷	B; T	I; E	SI,ML,AP	–	Cylinder (Ø 8 × 8 mm)	–	D	ε = 15%	E, σ _{max}	20; 519
	Brown & Ferguson ¹⁸	B	–	SI,ML,AP	–	Cube (5 × 5 mm)	–	D	F	E, σ _y	–; 800
	Chevalier et al. ¹⁹	B; T	–	SI	μCT, A	Cylinder (8 × 12 mm)	10; ε = 0.35%	ET	F	E, σ _y	3; 6
	Goulet et al. ²⁰	M	E	SI,ML,AP	μCT, A	Cube (8 × 8 mm)	10; σ _y /2	D	F	E, σ _{max}	4; 12
	Nazarian et al. ¹¹	T	I	7 directions	μCT	Cylinder (Ø5 × 10 mm)	7; –	ET	F	E, σ _y , ε _y	7; 47
	Matsuura et al. ²¹	B; T	I	SI	μCT	Cylinder (Ø8 × 12 mm)	12; ε = 0.35%	E	ε = 6%	E, σ _y , σ _{max}	185;146
	Morgan et al. ¹⁴	T	I	SI	A	Cylinder (Ø8 × 20 mm)	3; ε = 0.1% and 10; ε = 0.3%	E and D	ε = 0.5%	E, σ _y , ε _y	42; 33
	Homminga et al. ²²	B	I	SI	μCT	Cube (5 × 5 × 5 mm)	10; ε = 0.4%	D	ε = 15%	E, σ _y , ε _y	–;30
	Perilli et al. ¹⁵	B; M	I	SI	μCT	Cylinder (Ø 10 × 26 mm)	–	ET	F	σ _{max}	–; 50
	Öhman et al. ²³	B; M	I	SI, specified offset (20°)	μCT	Cylinder (Ø 10 × 26 mm)	–	ET	F	E, σ _{max}	–; 10
	Mazurkiewicz ²⁴	B; T *	–	SI	μCT	Cylinder (Ø 10 × 8.5 mm)	5; ε = 0.65%	D	F	σ _{max}	–;30
	Tassani et al. ⁷	M	I	SI	μCT	Cylinder (Ø 10 × 20 mm) ?	–	ET	F	σ _{max}	–, 25
Schoenfeld et al. ²⁵	B; T	–	SI, ML	?	Cylinder (Ø 4.5 × 9.5 mm)	–	D	F	σ _{max}	–; 30	
Distal femur	Goulet et al. ²⁰	M	E	SI	μCT, A	Cube (8 × 8 mm)	10; σ _y /2	D	F	E, σ _{max}	4; 39
Proximal tibia	Goulet et al. ²⁰	M	E	SI	μCT, A	Cube (8 × 8 mm)	10; σ _y /2	D	F	E, σ _{max}	4; 27
Vertebrae	Goulet et al. ²⁰	M	E	SI	μCT, A	Cube (8 × 8 mm)	10; σ _y /2	D	F	E, σ _{max}	4; 4
	Keaveney et al. ¹²	B; T; L	I	SI	A	Cylinder (Ø 8 × 35 mm)	10; ε = 0.3%	E	ε = 3%	E,	15; 15
	Keaveney et al. ²⁶	T;	–	SI	A	Cylinder (Ø 8.3 × 20...30 mm)	Varying preconditioning	E	ε = 4%	E, σ _{max}	15; 50
	Wegrzyn et al. ²⁷		I	SI,AP	μCT	Whole vertebral body	10; 50–100 N	E	F	Failure load, compressive stiffness	21;21
	Matsuura et al. ²¹	B; T	I	SI	μCT	Cylinder (Ø8 × 12 mm)	12; ε = 0.35%	E	ε = 6%	E, σ _y , σ _{max}	185; 307
Pelvis	Dalstra et al. ²⁸	B	CS	SI,ML,AP		Cube (6.5 × 6.5 mm)	5–10; ε = 0.8%	D	–	E	2; 57
Calcaneus	Matsuura et al. ²¹	B; T	I	ML	μCT	Cylinder (Ø 8 × 12 mm)	12; ε = 0.35%	E	ε = 6%	E, σ _y , σ _{max}	185;128
Radius	Matsuura et al. ²¹	B; T	I	ML	μCT	Cylinder (Ø8 × 12 mm)	12; ε = 0.35%	E	ε = 6%	E, σ _y , σ _{max}	185;162

Table 3. Survey of methodological designs of published literature regarding the compressive testing of human cancellous bone categorized over examined body parts. *A* Archimedic principle, *AP* anterior–posterior, *B* band saw, *C* clamps, *CS* coordinate-system, *D* direct contact, *E* embedding, *ET* endcap-technique, *F* failure of material, *I* imaging-methods, *L* lathe, *M* milling, *ML* medial–lateral, *SI* superior–inferior, *T* trephine, σ_{max} first maximum/ultimate stress, σ_y yield stress.

bone is underestimated by around 40%¹⁶. This systematic error can be reduced by embedding the trabecular ends using cyanoacrylate or casting resins^{12,30}. Another method is to glue thin metal plates to the sample ends with

cianoacrylate^{11,19,29}, as the adhesive hardens quickly and the plates ensure that the adhesive is not subjected to any transverse forces that could loosen the bond while testing. For a comparison of the examined groups a consistent method was carried out. But care must be taken when comparing the compressive modulus within other studies.

Before the actual destructive test, several loading and unloading cycles are usually performed. The advantages of this preconditioning are the setting of the material to compensate for alignment errors and the exclusion of possibly damaged specimens^{11,12}. Usually approx. 10 cycles are run between $\varepsilon = 0\%$ (lower limit) and $\varepsilon = 0.35\%$ (upper limit). In the present study one hysteresis loop was performed as preconditioning. The limits of the hysteresis were determined in a pre-test as it is prescribed in⁶.

Conclusion

For the fixation of the femoral heads during specimen extraction, generatively manufactured clamping jaws proved to be an effective instrument that enables fast and simple handling. Additionally it is cost-efficient in production, due to a more and more widespread use of desktop 3D-printers. The determination of bone density using separate discs from areas bordering the mechanical specimens worked well for the description of plateau and compressive stress. Consequently, a cost- and labour-intensive μ CT does not have to be carried out and the mechanical specimens remain unaffected and can be tested up to very large deformation ranges. The compact review of the extraction and testing methods from the literature illustrates the urgent need for standards regarding uniaxial compressive testing of human bone.

When comparing the different stages of osteoporosis based on the DEXA measurements, a general decrease in density and bone strength was observed with more pronounced disease progression. $\rho_{\text{app,distal}}$ was most suitable for predicting bone strength. No significant differences in mechanical properties (E , σ_{max} , σ_p) were found between osteopenic and osteoporotic bone.

The prediction of bone strength in clinical environment should be considered in a very sensitive way. The results suggest that already in the case of a known osteopenia, actions should be taken as they are applied in the case of osteoporosis (e.g. cementation of implants, imaging techniques).

Received: 25 January 2021; Accepted: 11 June 2021

Published online: 24 June 2021

References

- Krenn, V. *Pathologie des Bewegungsapparates* 2nd edn. (Walter de Gruyter GmbH Co.KG, 2012).
- Turner, C. H. & Burr, D. B. Basic biomechanical measurements of bone: A tutorial. *Bone* **14**, 595–608. [https://doi.org/10.1016/8756-3282\(93\)90081-K](https://doi.org/10.1016/8756-3282(93)90081-K) (1993).
- Keaveney, T. M. & Hayes, W. C. *Bone* (CRC Press. Inc., 1993).
- Oftadeh, R., Perez-Viloria, M., Villa-Camacho, J. C., Vaziri, A. & Nazarian, A. Biomechanics and mechanobiology of trabecular bone: a review. *J. Biomech. Eng.* **137**(1), 0108021–01080215. <https://doi.org/10.1115/1.4029176> (2015).
- Harrigan, T. P., Jasty, M., Mann, R. W. & Harris, W. H. Limitations of the continuum assumption in cancellous bone. *Memory Rik Huiskes*. **21**, 269–275. [https://doi.org/10.1016/0021-9290\(88\)90257-6](https://doi.org/10.1016/0021-9290(88)90257-6) (1988).
- DIN 50134:2008-10, *Prüfung von metallischen Werkstoffen_ - Druckversuch an metallischen zellularen Werkstoffen* (Beuth Verlag GmbH).
- Tassani, S., Ohman, C., Baleani, M., Baruffaldi, F. & Viceconti, M. Anisotropy and inhomogeneity of the trabecular structure can describe the mechanical strength of osteoarthritic cancellous bone. *J. Biomech.* **43**, 1160–1166. <https://doi.org/10.1016/j.jbiomech.2009.11.034> (2010).
- Halgrin, J., Chaari, F. & Markiewicz, É. On the effect of marrow in the mechanical behavior and crush response of trabecular bone. *J. Mech. Behav. Biomed. Mater.* **5**, 231–237. <https://doi.org/10.1016/j.jmbm.2011.09.003> (2012).
- Crandall, C. J. *et al.* A comparison of US and Canadian osteoporosis screening and treatment strategies in postmenopausal women. *J. Bone Miner. Res.* **34**, 607–615. <https://doi.org/10.1002/jbmr.3636> (2019).
- Carter, D. R. & Hayes, W. C. The compressive behavior of bone as a two-phase porous structure. *J. Bone Joint Surg.* **59**(7), 954–962 (1977).
- Nazarian, A., Muller, J., Zurakowski, D., Müller, R. & Snyder, B. D. Densitometric, morphometric and mechanical distributions in the human proximal femur. *Memory Rik Huiskes*. **40**, 2573–2579. <https://doi.org/10.1016/j.jbiomech.2006.11.022> (2007).
- Keaveney, T. M., Pinilla, T. P., Crawford, R. P., Kopperdahl, D. L. & Lou, A. Systematic and random errors in compression testing of trabecular bone. *J. Orthop. Res.* **15**, 101–110. <https://doi.org/10.1002/jor.1100150115> (1997).
- Ciarelli, T. E., Fyhrie, D. P., Schaffler, M. B. & Goldstein, S. A. Variations in three-dimensional cancellous bone architecture of the proximal femur in female hip fractures and in controls. *J. Bone Miner. Res.* **15**, 32–40. <https://doi.org/10.1359/jbmr.2000.15.1.32> (2000).
- Morgan, E. F. & Keaveney, T. M. Dependence of yield strain of human trabecular bone on anatomic site. *J. Biomech.* **34**, 569–577. [https://doi.org/10.1016/S0021-9290\(01\)00011-2](https://doi.org/10.1016/S0021-9290(01)00011-2) (2001).
- Perilli, E. *et al.* Dependence of mechanical compressive strength on local variations in microarchitecture in cancellous bone of proximal human femur. *J. Biomech.* **41**, 438–446. <https://doi.org/10.1016/j.jbiomech.2007.08.003> (2008).
- Linde, F. & Hvid, I. The effect of constraint on the mechanical behaviour of trabecular bone specimens. *J. Biomech.* **22**, 485–490. [https://doi.org/10.1016/0021-9290\(89\)90209-1](https://doi.org/10.1016/0021-9290(89)90209-1) (1989).
- Martens, M., van Audekercke, R., Delpont, P., de Meester, P. & Mulier, J. C. The mechanical characteristics of cancellous bone at the upper femoral region. *Memory Rik Huiskes*. **16**, 971–983. [https://doi.org/10.1016/0021-9290\(83\)90098-2](https://doi.org/10.1016/0021-9290(83)90098-2) (1983).
- Brown, T. D. & Ferguson, A. B. Mechanical property distributions in the cancellous bone of the human proximal femur. *Acta Orthop. Scand.* **51**, 429–437. <https://doi.org/10.3109/17453678008990819> (1980).
- Chevalier, Y., Pahr, D., Allmer, H., Charlebois, M. & Zysset, P. Validation of a voxel-based FE method for prediction of the uniaxial apparent modulus of human trabecular bone using macroscopic mechanical tests and nanoindentation. *J. Biomech.* **40**, 3333–3340. <https://doi.org/10.1016/j.jbiomech.2007.05.004> (2007).
- Goulet, R. W. *et al.* The relationship between the structural and orthogonal compressive properties of trabecular bone. *J. Biomech.* **27**, 375–389. [https://doi.org/10.1016/0021-9290\(94\)90014-0](https://doi.org/10.1016/0021-9290(94)90014-0) (1994).
- Matsuura, M., Eckstein, F., Lochmuller, E.-M. & Zysset, P. K. The role of fabric in the quasi-static compressive mechanical properties of human trabecular bone from various anatomical locations. *Biomech. Model. Mechanobiol.* **7**, 27–42. <https://doi.org/10.1007/s10237-006-0073-7> (2008).

22. Homminga, J. *et al.* Cancellous bone mechanical properties from normals and patients with hip fractures differ on the structure level, not on the bone hard tissue level. *Bone* **30**, 759–764. [https://doi.org/10.1016/S8756-3282\(02\)00693-2](https://doi.org/10.1016/S8756-3282(02)00693-2) (2002).
23. Ohman, C. *et al.* Mechanical testing of cancellous bone from the femoral head: experimental errors due to off-axis measurements. *J. Biomech.* **40**, 2426–2433. <https://doi.org/10.1016/j.jbiomech.2006.11.020> (2007).
24. Mazurkiewicz, A. Influence of the trabecular bone structure indicators on its static and fatigue strengths. In *Danubia-Adria Symposium on Advances in Experimental Mechanics* (ed. F. Cosmi) (EUT Edizioni Università di Trieste, 2017).
25. Schoenfeld, C. M., Lautenschlager, E. P. & Meyer, P. R. Mechanical properties of human cancellous bone in the femoral head. *Med. Biol. Eng.* **12**, 313–317. <https://doi.org/10.1007/BF02477797> (1974).
26. Keaveny, T. M., Wachtel, E. F. & Kopperdahl, D. L. Mechanical behavior of human trabecular bone after overloading. *J. Orthop. Res.* **17**, 346–353. <https://doi.org/10.1002/jor.1100170308> (1999).
27. Wegrzyn, J. *et al.* Role of trabecular microarchitecture and its heterogeneity parameters in the mechanical behavior of ex vivo human L3 vertebrae. *J. Bone Miner. Res.* **25**, 2324–2331. <https://doi.org/10.1002/jbmr.164> (2010).
28. Dalstra, M., Huiskes, R., Odgaard, A. & van Erning, L. Mechanical and textural properties of pelvic trabecular bone. *J. Biomech.* **26**, 523–535. [https://doi.org/10.1016/0021-9290\(93\)90014-6](https://doi.org/10.1016/0021-9290(93)90014-6) (1993).
29. Rincon-Kohli, L. & Zysset, P. K. Multi-axial mechanical properties of human trabecular bone. *Biomech. Model Mechanobiol.* **8**, 195–208. <https://doi.org/10.1007/s10237-008-0128-z> (2009).
30. Linde, F., Hvid, I. & Madsen, F. The effect of specimen geometry on the mechanical behaviour of trabecular bone specimens. *Memory Rik Huiskes.* **25**, 359–368. [https://doi.org/10.1016/0021-9290\(92\)90255-Y](https://doi.org/10.1016/0021-9290(92)90255-Y) (1992).
31. Rho, J. Y., Hobatho, M. C. & Ashman, R. B. Relations of mechanical properties to density and CT numbers in human bone. *Med. Eng. Phys.* **17**, 347–355. [https://doi.org/10.1016/1350-4533\(95\)97314-F](https://doi.org/10.1016/1350-4533(95)97314-F) (1995).
32. Turner, C. H., Cowin, S. C., Rho, J. Y., Ashman, R. B. & Rice, J. C. The fabric dependence of the orthotropic elastic constants of cancellous bone. *J. Biomech.* **23**, 549–561. [https://doi.org/10.1016/0021-9290\(90\)90048-8](https://doi.org/10.1016/0021-9290(90)90048-8) (1990).
33. Keaveny, T. M., Morgan, E. F., Niebur, G. L. & Yeh, O. C. Biomechanics of trabecular bone. *Annu. Rev. Biomed. Eng.* **3**, 307–333. <https://doi.org/10.1146/annurev.bioeng.3.1.307> (2001).
34. Goldstein, S. A., Goulet, R. & McCubbrey, D. Measurement and significance of three-dimensional architecture to the mechanical integrity of trabecular bone. *Calcif Tissue Int.* **53**, S127–S133. <https://doi.org/10.1007/BF01673421> (1993).
35. Gibson, L. J. The mechanical behaviour of cancellous bone. *J. Biomech.* **18**, 317–328. [https://doi.org/10.1016/0021-9290\(85\)90287-8](https://doi.org/10.1016/0021-9290(85)90287-8) (1985).
36. Galante, J., Rostoker, W. & Ray, R. D. Physical properties of trabecular bone. *Calcif. Tissue Res.* **5**, 236–246. <https://doi.org/10.1007/BF02017552> (1970).

Author contributions

F.M., C.N, C-E.H., W-G.D. and S.S. designed the study. F.M., C.N wrote the manuscript. F.M. and J-P.F. did the laboratory experiments. All authors reviewed the manuscript.

Funding

Open Access funding enabled and organized by Projekt DEAL. We acknowledge support from Leipzig University for Open Access Publishing.

Competing interests

The authors declare no competing interests.

Additional information

Supplementary Information The online version contains supplementary material available at <https://doi.org/10.1038/s41598-021-92685-z>.

Correspondence and requests for materials should be addressed to F.M.

Reprints and permissions information is available at www.nature.com/reprints.

Publisher's note Springer Nature remains neutral with regard to jurisdictional claims in published maps and institutional affiliations.



Open Access This article is licensed under a Creative Commons Attribution 4.0 International License, which permits use, sharing, adaptation, distribution and reproduction in any medium or format, as long as you give appropriate credit to the original author(s) and the source, provide a link to the Creative Commons licence, and indicate if changes were made. The images or other third party material in this article are included in the article's Creative Commons licence, unless indicated otherwise in a credit line to the material. If material is not included in the article's Creative Commons licence and your intended use is not permitted by statutory regulation or exceeds the permitted use, you will need to obtain permission directly from the copyright holder. To view a copy of this licence, visit <http://creativecommons.org/licenses/by/4.0/>.

© The Author(s) 2021